A Merging Solution for Close-Range DEMs to Optimize Surface Coverage and Measurement Resolution

Stephane Bertin, Heide Friedrich, and Patrice Delmas

Abstract

The process of efficient and effective DEM merging is increasingly becoming more important. To allow DEM analysis for features of different scales, an increase in surface coverage cannot result in reduced measurement resolution. It is thus inevitable that merging individual high-resolution DEMs will become common practice for applications such as hydraulic roughness studies for fluvial surfaces. This paper presents an efficient and effective merging solution, whereby accurate co-registration of individual DEMs collected from consistent viewpoints and standard averaging for overlapping elevations ensure seamless merging. The presented method is suitable for DEMs collected using any measurement technology, as long as individual DEMs overlap and are arranged on regular grids. The merging solution is applied to the study of a laboratory gravel bed measured with vertical stereo photogrammetry at the grain scale (>10^6 points/m2). We show that the approach can be integrated into the DEM collection workflow at the design stage, which optimizes the measurement performance. We present how resampling before merging can be beneficial to keep data handling requirements practical, whilst ensuring accurate surface representation. Finally, the effect of scale variation is studied, showing that seamless merging applies to DEMs with variable resolution.

Introduction

Problem Statement

Regularly gridded digital elevation models (DEMs) to survey areas of interest in both the laboratory and the field are commonly used in fluvial hydraulics and the Earth sciences. Often, a compromise has to be found between surface coverage and measurement resolution. This is particularly true when DEMs are obtained by photogrammetric means due to the finite sensor size, and this also holds for other common measurement techniques.

The trade-off between surface coverage and measurement resolution in the photogrammetric application can be demonstrated using the standard projective formulae, also commonly known as the pin-hole camera model. For a vertical stereo-photogrammetric configuration between two identical cameras, the optical axes are parallel to each other and perpendicular to the baseline. For such an arrangement, the common field of view (CFoV) between the two images forming a stereo pair is enlarged, whereby 3D information is extracted by increasing the camera-to-object distance, Z:

$$\mathrm{CFoV_W} = \frac{Zw}{f} - b \tag{1}$$

$$\mathrm{CFoV_H} = \frac{Zh}{f} \tag{2}$$

where f is the camera focal length in pixel, b is the constant baseline distance, w and h are the width and the height of the cameras' sensor in pixel, respectively, whilst the indices $_W$ and $_H$ represent the directions parallel and perpendicular to the baseline. Values are in metric units unless specifically stated. The pixel size in the object space, S_p, which is the minimum usable DEM grid size, and the theoretical depth resolution, δ_Z, also called the minimum measurable depth, are related to the camera-to-object distance as following:

$$S_p = \frac{Zp}{f} \tag{3}$$

$$\delta_Z = \frac{Z^2 p}{bf - Zp} \tag{4}$$

where p is the camera pixel size. One can see that by increasing Z, both the horizontal (i.e., pixel size in the object space) and the depth resolution will deteriorate.

Increasingly, studies' regions of interest often exceed the minimal measurement resolution required to record the surface with solely one DEM. To address this issue, smaller DEMs (thus of higher measurement resolution) can be recorded and merged together to produce a DEM that has both, acceptable surface coverage and measurement resolution. In the literature, DEM merging is also generally referred to as DEM mosaicking, DEM stitching, and more generally data fusion. Examples of applications in the Earth sciences can be found in the work of Stojic *et al.* (1998), Butler *et al.* (2001), Chandler *et al.* (2002 and 2001), Wackrow (2008) and Marzahn *et al.* (2012).

The Challenges

1. Visible seams can affect merged DEMs, degrading the measurement accuracy and potentially impacting parameters extracted from the DEMs (James *et al.*, 2007). Those seams are caused by horizontal and/or vertical shifts between individual DEMs, where co-registration was insufficient.
2. The integration of the merging approach into the DEM collection workflow requires two new parameters: (a) the number of DEMs used for the merging, and (b) the overlap between the DEMs. The two parameters are

Stephane Bertin and Heide Friedrich are with the Department of Civil and Environmental Engineering, Faculty of Engineering, The University of Auckland, Private Bag 92019, Auckland 1142, New Zealand (s.bertin@ymail.com).

Patrice Delmas is with the Department of Computer Science, The University of Auckland, Private Bag 92019, Auckland 1142, New Zealand.

Photogrammetric Engineering & Remote Sensing
Vol. 82, No. 1, January 2016, pp. 31–40.
0099-1112/16/31–40

doi: 10.14358/PERS.83.1.31

inter-dependent and their optimization is critical to the global DEM quality and process efficiency.

3. Data handling can be challenging after merging (Barazzetti *et al.*, 2013). A fit-for-purpose analysis has to be undertaken before data recording to ensure the chosen measurement resolution suits the tasks ahead. This pre-analysis is becoming more critical, as it reduces the computing and data storage demands, whilst it also ensures appropriate data recording. Correct resampling might allow for more efficient data handling, without losing critical information.

State of the Art

Specialist photogrammetric and GIS software packages, such as IMAGINE Photogrammetry® (previously LPS/OrthoMAX) by Leica Geosystems, ENVI®, and Esri's ArcGIS®, comprise a built-in DEM merging function. Techniques commonly referred to as "feathering" are used. Weighted-averaging is generally used to overlap data. By smoothing ("feathering") the overlap region, any inconsistencies at the boundaries are reduced. However, it is important to note that this process does not remove the systematic errors that caused the discontinuities in the first place (Costantini *et al.*, 2006).

Gallant and Austin (2009) used Esri's "mosaic" function to merge land and bathymetric datasets obtained in South Australia. They showed that merging could be automated, but only by relying on the DEMs overlap. Otherwise, the process was described as "manually intensive, requiring a great deal of intervention, judgement, analysis and editing." Stojic *et al.* (1998), Chandler *et al.* (2001 and 2002) and Wackrow (2008) used OrthoMAX/LPS to merge overlapping DEMs obtained with close-range stereo photogrammetry. Wackrow (2008) reportedly used an overlap of 60 percent the size of the input DEMs, which was the same overlap distance between two images forming a stereo pair. Despite such a high data redundancy, discontinuities were still clearly visible after DEM merging (Stojic *et al.*, 1998; Wackrow, 2008). Reasons for the failure were not discussed. Registration errors were pointed out as being responsible for elevation discontinuities after merging land and bathymetric raster DEMs of Tampa Bay, Florida (Medeiros *et al.*, 2011). Postprocessing with ArcGIS® was necessary to reduce the significance of the seam. Marzahn *et al.* (2012) used LPS for the measurement of soil surface roughness, but preferred a self-programmed merging technique to increase the surface coverage in their study. The technique was simply described as "a postprocessing step using image matching techniques," requiring a 30 percent overlap between successive DEMs to merge. Unfortunately, the merging technique, results and evaluation were not presented.

With the recent availability of free-to-use wide-area (also called global) DEMs, such as those obtained using Advanced Spaceborne Thermal Emission and Reflection Radiometer (ASTER) and Shuttle Radar Topographic Mission (SRTM), data fusion is receiving growing attention in the scientific community. In those cases, DEMs were generally collected using different techniques, and subsequent data fusion aims to use redundant information to obtain a more accurate surface estimation (Papasaika *et al.*, 2011). Although the motivations for data fusion are not the same as for data merging, some data fusion strategies can be transferred to DEM merging. Costantini *et al.* (2006) proposed a data fusion algorithm to merge large-scale DEMs of a test site in central Italy, originating from various data sources. Similar to other data fusion techniques (Papasaika *et al.*, 2011; Papasaika *et al.*, 2008; Schindler *et al.*, 2011; Tran *et al.*, 2014), their method exploits the redundant information contained in the area of overlap between different DEMs in order to reduce the horizontal and vertical systematic errors. This resembles a 3D co-registration of the individual DEMs, an essential step for creating a seamless, merged product (Gesch and Wilson, 2002). After alignment of the individual DEMs, redundant elevation data are processed by means of averaging. Weighted-averaging is the favored method when various data sources are used. Weights can be determined based on the theoretical or measured accuracy of the input DEMs, as well as characteristics of the surface, such as slope and roughness.

Novel Structure-from-Motion (SfM) and Multi-View Stereo (MVS) allow for DEM reconstruction from more than two images, and therefore would be a viable solution to the problem investigated in this study (Dowling *et al.*, 2009; Fonstad *et al.*, 2013; James and Robson, 2014; Javernick *et al.*, 2014; Ouédraogo *et al.*, 2014; Stumpf *et al.*, 2015; Westoby *et al.*, 2012). However, SfM/MVS currently lack the capability of traditional close-range stereo photogrammetry in recording high-quality small-scale DEMs, as is necessary for grain-scale fluvial roughness characterization. Furthermore, it has been shown that DEMs collected with these techniques may suffer from large non-linear distortions (the so-called "dome effect") due to inadequate lens distortion calibration (Fonstad *et al.*, 2013; Ouédraogo *et al.*, 2014); a drawback that has been resolved in traditional stereo photogrammetry (Bertin *et al.*, 2015; Wackrow, 2008).

Motivations and Aims

The use of non-proprietary close-range digital photogrammetry is increasingly becoming more common for studies in fluvial hydraulics and the Earth sciences (Bertin and Friedrich, 2014; Bertin *et al.*, 2014; Bouratsis *et al.*, 2013; Musumeci *et al.*, 2013). We previously reported on our development of a non-proprietary stereo-photogrammetric setup capable of recording fluvial surfaces at the grain scale, characterized by DEMs with 0·25 mm sampling distance and sub-millimeter accuracy (see Bertin *et al.* (2014 and 2015) for a detailed evaluation of the technique). We also showed that the same setup can be used for through-water recordings, with water depths up to 200 mm (Bertin *et al.*, 2013).

The present paper unveils an efficient and effective seamless DEM merging method, which supports our high-resolution stereo-photogrammetric application, and allows us to increase the surface coverage, and therefore the range of potential applications, without reducing DEM quality. Our proposed merging method is computationally efficient and can be adapted to any DEM, independent on the measurement recording technique. The only prerequisite is the existence of DEMs' overlap and regular grid arrangement, both easily satisfied in practice.

Our DEM merging solution is applied to the study of laboratory water-worked gravel-beds. Previous studies on the fluvial microtopography and grain-scale roughness, using either close-range digital photogrammetry or terrestrial laser scanning (TLS), were limited to small surfaces (0·25 m^2 and less), in order to guarantee efficient recording and sub-millimeter resolution. The present paper shows that DEM merging enables the recording and subsequent analysis of large-scale micro-topographic information. This new process we present herewith will now allow researchers to advance our fundamental fluvial knowledge by fusing grain-scale and bedform roughness in both laboratory and field studies.

Measurement Environment and Instrumentation

A hydraulic flume (19 m long, 0.45 m wide, and 0.5 m deep) is used for our gravel-bed studies. The setup is described previously (Bertin and Friedrich, 2014; Bertin *et al.*, 2014; Heays *et al.*, 2014). A gravel bed (0.71 mm <d <35 mm, where d is the intermediate axis of the sediment particles) was prepared in a 950 mm long full-width test section, located 14 m from the flume inlet. The gravel bed was water-worked at a constant flow rate (84 L/s) until the sediment surface was in static equilibrium. During water-work, fine sediment at the surface was transported downstream, uncovering coarser particles, which then formed the so-called "armor layer". After

water-work, particles of less than 5 mm in size were scarcely represented on the gravel-bed surface.

Two Nikon D5100 cameras in stereo, with 16.2 Mpixel complementary metal oxide semiconductor (CMOS) sensors (4,928 × 3,264 pixels) and Nikkor 20 mm fixed-focus lenses, were used for the image acquisition of the dry gravel bed. The setup was installed on a carriage, which can move along the hydraulic flume and allowed for continuous acquisition of overlapping stereo-pair sequences. To minimize the presence of occlusions (also known as "dead ground"), a recurrent problem on rough surfaces (Bertin *et al.*, 2014; Chandler *et al.*, 2002; Chandler *et al.*, 2001), and simplify image rectification, a standard vertical stereo-photogrammetric configuration was used: optical axes parallel to each other and perpendicular to the baseline. Even lighting of the test section was ensured (Bertin *et al.*, 2014).

Data processing was performed on an Alienware laptop with Intel core CPU @ 2.20 GHz, 8 GB memory and MATLAB® 2013b.

General DEM Collection Workflow

Figure 1 summarizes the general workflow developed and evaluated in Bertin *et al.* (2014 and 2015) and used in this study to reconstruct a 2.5D DEM from a stereo pair. The region of interest is restricted by the CFoV formed by the two images. Before presenting our new integrated DEM merging strategy, we briefly summarize the main steps of our previous general DEM collection workflow, to allow for a comparison later on.

The design of the setup is the first step of the workflow. The aim is to find the minimum camera-to-object distance that is needed to ensure the CFoV covers the region of interest (Equations 1 and 2). The measurement resolution is dependent on the region of interest and the cameras' sensor size (Equations 3 and 4). To measure a gravel bed (950 × 400 mm) with one DEM (i.e., without merging) and a 5 percent margin all around, the cameras were installed at a vertical distance of 1,100 mm above the section. A baseline of 250 mm was used, based on experimental heuristics. This results in a pixel size and a theoretical depth resolution, at the distance of the gravel bed, of 0·26 mm and 1.15 mm, respectively (Table 1).

After careful preparation of the setup, several stereo photographs of a flat checkerboard, necessary for accurate camera calibration and pose determination, and one stereo pair of the gravel bed, were recorded. The cameras were operated in manual mode, using a combination of f/8 aperture, ISO 200 and 1/20 s shutter speed. Data processing consisted in (a) determining the camera calibration (e.g., principal distance, principal point, and five-coefficient lens distortion) and pose (3D rotation and translation between the two camera) parameters using the calibration images and Bouguet's camera calibration toolbox for MATLAB® (Bouguet, 2010; Bouratsis *et al.*, 2013; Bruno *et al.*, 2011); (b) rectifying the gravel-bed stereo pair to epipolar geometry (Fusiello *et al.*, 2000), corresponding pixels being ideally on a same scanline; (c) scanline-based pixel-to-pixel stereo matching on the rectified Red/Green/Blue (RGB) stereo pair of the gravel bed using the symmetric dynamic programming stereo (SDPS) algorithm (Gimel'farb, 2002), whereby occluded points are interpolated based on the assumption of a continuous surface, leaving no voids in the DEM (see Bertin *et al.* (2015) for more details on the calibration and stereo matching engine); (d) point cloud extraction using projective geometry and the calibration data; and (e) interpolation of the point cloud onto an orthogonal grid using MATLAB®. The gravel bed DEM (950 × 400 mm) was interpolated onto a grid with 0·26 mm spacing (Table 1), consistent with the theoretical sampling distance achievable for this setup.

TABLE 1. SUMMARY OF THE STEREO-PHOTOGRAMMETRIC SETUPS DESIGNED TO MEASURE THE TEST SECTION (950 × 400 MM). ALL VALUES WERE THEORETICALLY DETERMINED USING PROJECTIVE GEOMETRY AND THE ROUNDED CAMERA-TO-OBJECT DISTANCE. ACTUAL VALUES MAY DEVIATE MINIMALLY BECAUSE OF THE DIFFICULTY IN PRACTICE TO ACCURATELY SET THE CAMERAS "FLYING-HEIGHT" AND CAMERAS BASELINE.

	Without merging	With merging
Baseline (mm)	250	250
Number of DEMs to cover test section (-)	1	3
Overlap between adjacent DEMs (% of DEM size)	N.A	30
Translation to apply to setup (mm)	N.A	277
Rounded camera-to-object distance (mm)	1098	581
Margin around DEM (% of DEM size)	5	5
$CFoV_W \times CFoV_H$ (mm)	1045 × 860	435 × 455
Overlap between two images forming a stereo pair (%)	81	63
Pixel size on the surface (mm)	0·26	0·14
Theoretical depth resolution (mm)	1·15	0·32

N.A stands for non-applicable

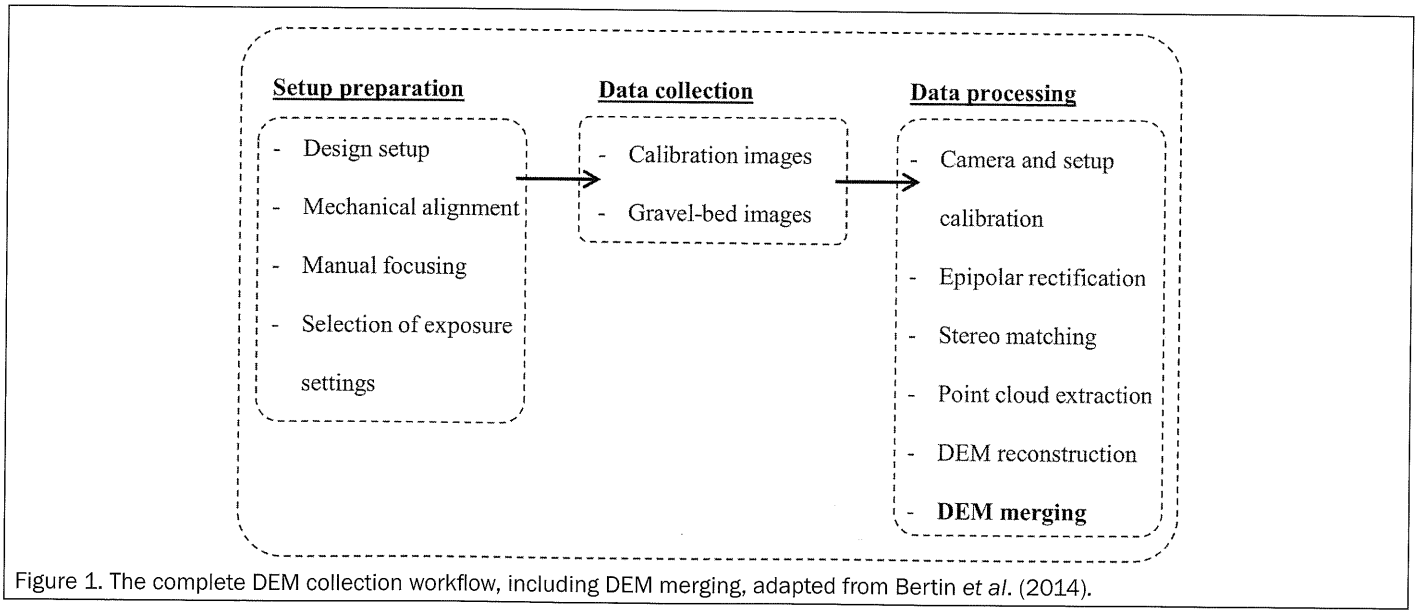

Figure 1. The complete DEM collection workflow, including DEM merging, adapted from Bertin *et al.* (2014).

Integrated DEM Merging Strategy

Adapted Stereo-Photogrammetric Design

In contrast to merging methods used in commercial software as standalone tools, an integrated DEM merging strategy requires the identification of the number of DEMs needed for merging and the overlap between individual DEMs. Those two parameters need to be accounted for in the stereo-photogrammetric design for optimum results. Assuming the same area has to be covered, with a need to improve the theoretical depth resolution from 1.15 mm to less than 0.5 mm to guarantee reliable roughness measures, the baseline can be kept constant, while merging three individual DEMs (Table 1).

The quality of the merged DEM and the process efficiency are directly affected by the number of individual DEMs and the overlap between them. The existence of an overlap was already previously shown to be critical to DEM merging (Gallant and Austin, 2009; Streutker *et al.*, 2011). Marzahn *et al.* (2012) used an overlap of 30 percent of the size of an individual DEM and our preliminary experiments resulted in choosing the same value for the present study. We could not find any other overlap threshold information in the literature. We found that 30 percent allows for accurate co-registration of DEMs and minimizes the number of DEMs to cover the test section, assuming both requirements are equally important.

Table 1 summarizes the characteristics of the setup designed to obtain one merged DEM of the gravel bed (950 × 400 mm), using three overlapping individual DEMs, each with a 5 percent margin. The width of the flume meant that only one row of DEMs was acquired, but the process we present can be extended to merge DEMs in both axes. Based on the design formulae (Equations 1 and 2), the cameras were placed approximately 581 mm above the test section. The pixel size on the gravel bed and the theoretical depth resolution were 0.14 and 0.32 mm, respectively (Table 1). Data collection and processing were similar to the general DEM collection workflow, with the exception that three stereo pairs of the gravel bed were recorded and processed. After the acquisition of one stereo pair, the setup was translated by 277 mm to allow a 30 percent overlap with the next stereo pair (Figure 2). The individual DEMs can then be interpolated onto a regular grid with 0.14 mm spacing.

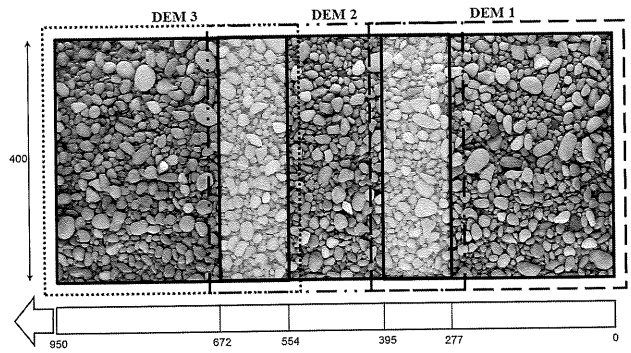

Figure 2. Description of the setup, specifically designed to obtain a merged DEM of size 950 × 400 mm from three individual DEMs overlapping at 30 percent. The dashed lines indicate the margin, i.e., at least 5 percent.

3D Co-Registration and Merging

Given two reconstructed overlapping DEMs, herewith referred to as DEM-1 and DEM-2, the horizontal and vertical shifts between them are numerically estimated using a self-programmed MATLAB® function. The outcome of the computation is the line's coordinates in DEM-2 where stitching is to occur (i.e., at the front of the overlap area), and the bi-linear surface, which represents the vertical shift between the two DEMs.

To perform the horizontal registration or alignment between DEM-1 and DEM-2, DEM-2 is moved horizontally with increments equal to the grid size by means of translations until best match. Hence, one can see that the horizontal registration precision depends on the DEM resolution. To determine the best match iteratively and together perform the vertical registration, the information at the overlap between DEM-1 and DEM-2 (i.e., the residual map) is utilized to compute by least-squares the bi-linear surface that represents best the vertical shift between DEM-1 and DEM-2. Such a trend can be caused by a change in orientation of the setup between the acquisitions of the two DEMs (hence a bi-linear surface). Depending on how the residual map is produced, the calculated trend is then either removed or added to DEM-2. We propose to use the smallest mean unsigned (or absolute) error (MUE) between the two DEMs, after vertical alignment, as the criterion for best match.

Finally, the areas of DEM overlap are averaged. If individual DEMs are obtained from the same survey, as is the case for the present study, we show that standard averaging can be used.

Results

Figure 3 shows three individual DEMs, altogether covering the test section. One can see the overlap between two adjacent DEMs, approximately 30 percent the DEM size. Using a small

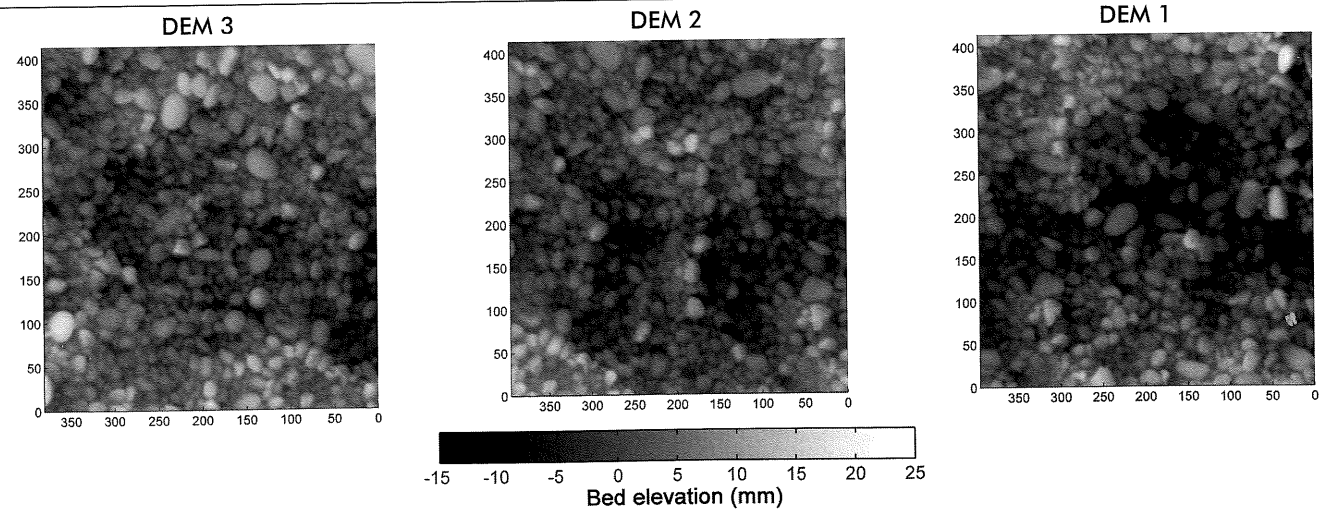

Figure 3. Individual DEMs (395 × 415 mm) after margin removal, altogether covering the entire region of interest. The sampling distance is 0·25 mm and the theoretical depth resolution is 0·32 mm.

camera-to-object distance during image acquisition (~581 mm) ensures that individual DEMs accurately represent the gravel-bed surface. Individual particles are clearly defined, which is necessary to undertake grain-scale roughness analyses, such as monitoring changes in the particles' slope and orientation with water-work.

Large data files for individual DEMs will make merging of those DEMs computationally expensive, and often not feasible (Barazzetti *et al.*, 2013). Therefore we studied the effect resampling has on the merged DEM. Here, DEM resampling interpolates a DEM on a less dense grid system. In Bertin *et al.* (2014) we showed the effect of raw point cloud interpolation onto regular grids with different spacing using a ground truth. The benchmark grid size we tested was 0·25 mm for that study. We found that raw point clouds should be interpolated onto grids with spacing closely matching the original point data spacing in order to reduce smoothing artifacts. In order to be able to compare the present results with previously studied benchmarks, we also restrict the minimal grid size to 0·25 mm for this study, although the individual DEMs would allow us to go as low as 0.14 mm (i.e., a DEM grid spacing matching the pixel size at the distance of the gravel bed). Figure 4 shows the results of resampling for an individual DEM onto coarser grids. The middle DEM (DEM-2) is taken as an example. Four tests were performed: resampling the original DEM characterized by a 0·25 mm sampling distance, onto grids with spacing 0.5 mm, 0.75 mm, 1 mm, and 1.5 mm, respectively. The internal reliability of the resampled DEMs is assessed to decide if DEM resampling before merging is suitable (Figure 4). The point-wise mean unsigned error (MUE) and standard deviation of error (SDE) were computed after differentiation of the resampled DEMs with the original DEM:

$$\mathrm{MUE} = \frac{\sum_{i=1}^{n} |r_i - o_i|}{n} \tag{5}$$

$$SDE = \sqrt{\frac{\sum_{i=1}^{n} \left[(r_i - o_i) - \overline{(r_i - o_i)} \right]^2}{n}} \tag{6}$$

where r_i = resampled elevations; o_i = original elevations.

Figure 4 shows that DEM resampling impacted small features, particles' edges and gaps especially. In this application, resampling was considered to have a minor effect up to a 1 mm grid, after which SDE passed the 0.1 mm mark. Individual DEMs were therefore resampled onto a grid with 1 mm spacing before merging. It ensured a computationally efficient merging and handling of the resulting DEM, with minimum impact on the recorded topography.

Figure 5 shows the composite DEM after seamless merging. It is clearly seen that standard averaging of the overlap

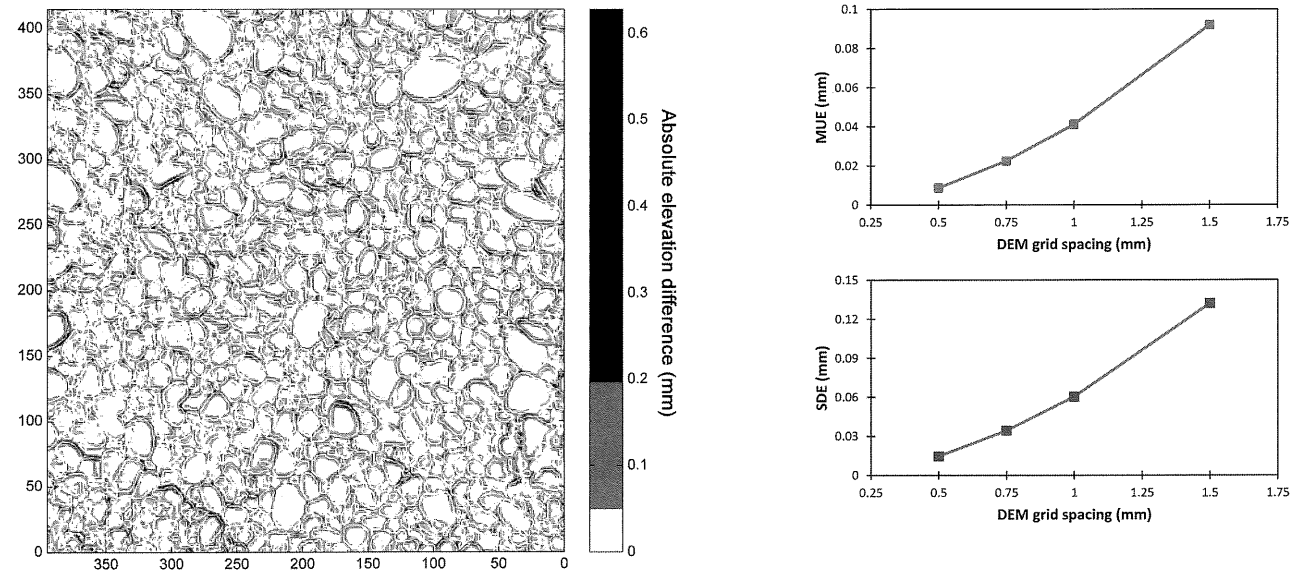

Figure 4. Internal reliability of DEM resampling, i.e., point-wise comparison between DEMs after resampling and original DEM, characterized by 0·25 mm sampling distance. Comparison was performed on the original grid, i.e., 0·25 mm. (Left) DEM of absolute difference between the DEM resampled onto a grid with 1 mm spacing and the original DEM (Right) Internal reliability statistics.

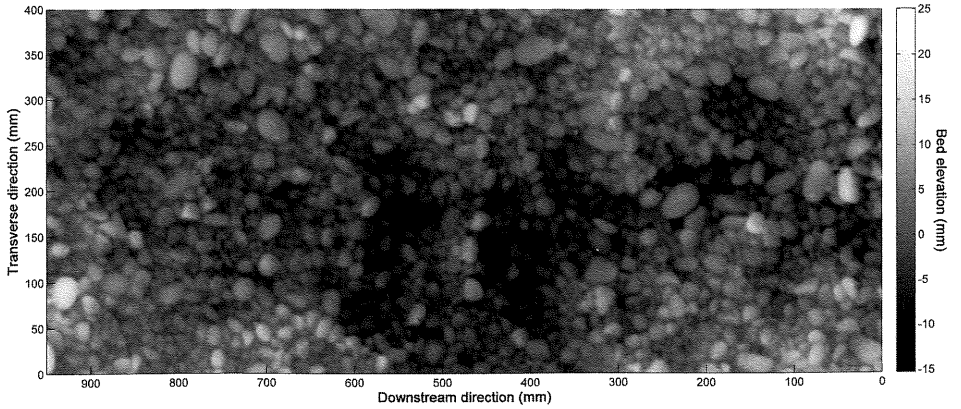

Figure 5. Final DEM after merging. The sampling distance is 1 mm and the theoretical depth resolution is 0·32 mm.

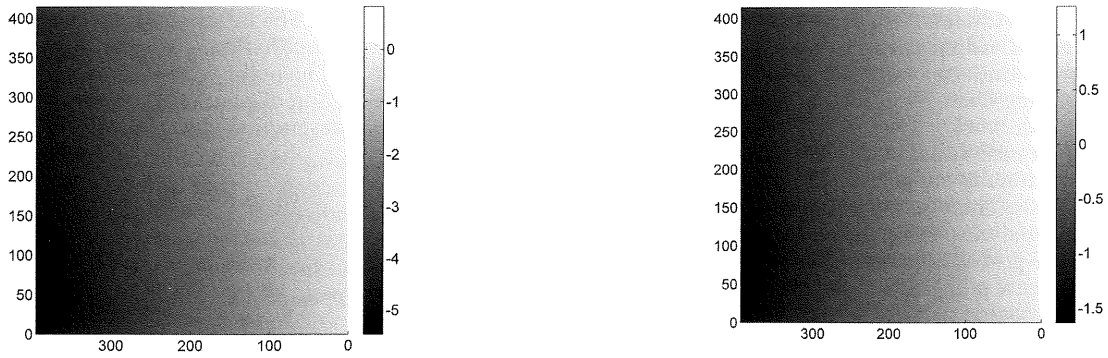

Figure 6. Trends in mm removed during vertical registration of overlapping DEMs. A linear surface is fitted to the residual maps (118 × 415 mm) using the least-squares method, which is then interpolated over the size of the DEM (395 × 415 mm). The sampling distance is 1 mm.

between adjacent DEMs does not blur the recorded topography because of the consistent DEM quality and precise alignment. Co-registration prior to merging is essential. If not applied, vertical shifts at the intersection between individual DEMs can cause elevation disparities of up to 1 mm, and changes in slope of up to 1.6 percent, as observed over the length of one DEM (Figure 6).

As merging is performed to capture information that cannot be obtained by a single measurement, it is often not feasible to have a suitable ground truth to evaluate the merging success. For our stereo-photogrammetric application, the accuracy and precision of an individual DEM was evaluated previously, by measuring a 3D-printed ground truth resembling a water-worked gravel bed (Bertin *et al.*, 2014). In the latter study, comparison of measured and "truth" data resulted in a distribution of DEM errors characterized by a statistical accuracy and precision of 0·43 mm (MUE) and 0·62 mm (SDE), respectively.

The co-registration of individual DEMs can be assessed without a ground truth. Figure 7 shows the two residual maps after co-registration of DEM-1 and DEM-2, and DEM-2 and DEM-3, respectively. Both residual maps are characterized by a zero mean error (ME) and no blur, suggesting the horizontal registration precision of 1 mm (i.e., the DEM grid size) was suitable for effective merging. Furthermore, no significant trend is observed after co-registration, which concludes that any DEM misalignment prior to merging was correctly removed during co-registration. We also recommend manual checking of the combined longitudinal elevation profile (Figure 8), which can be used as indication of accurate 3D co-registration between individual DEMs.

As comparison, the non-merged DEM, obtained using a single stereo pair, is presented in Figure 9. The effect of

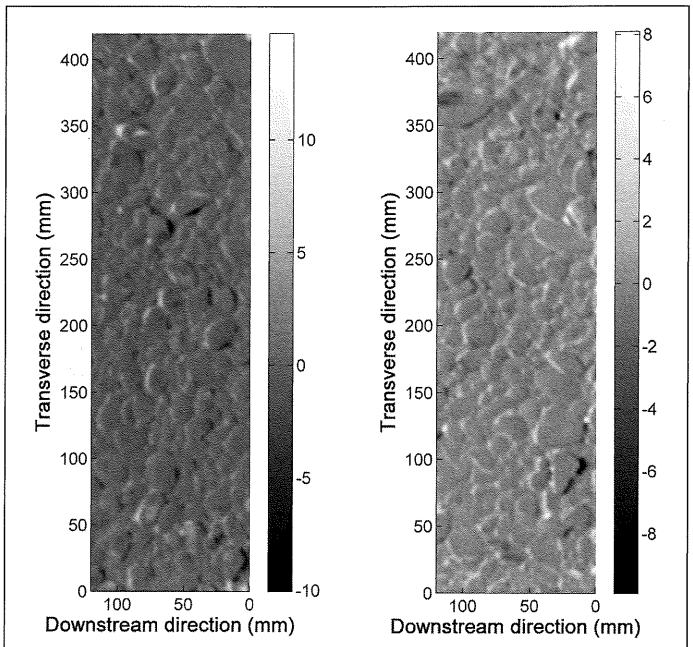

Figure 7. Residual maps, i.e., elevation difference in mm between adjacent DEMs after co-registration. The sampling distance is 1 mm.

increased theoretical depth resolution (from 0.32 mm to 1.15 mm) and pixel size (from 0.14 mm to 0·26 mm), caused by a larger camera-to-object distance (from 581 mm to 1,098 mm) during image acquisition, is clearly visible. The non-merged DEM (Figure 9) loses sharpness and lacks detailed information

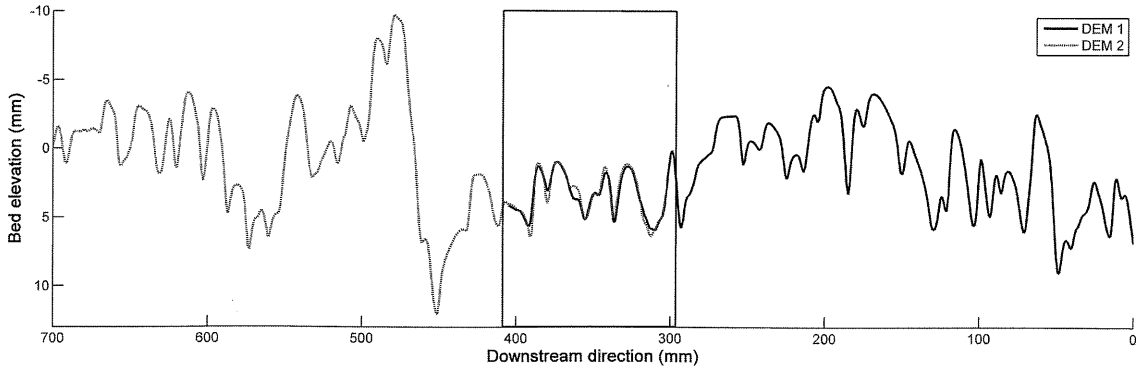

Figure 8. Longitudinal elevation profile, showing the area of overlap between DEM-1 and DEM-2, after co-registration.

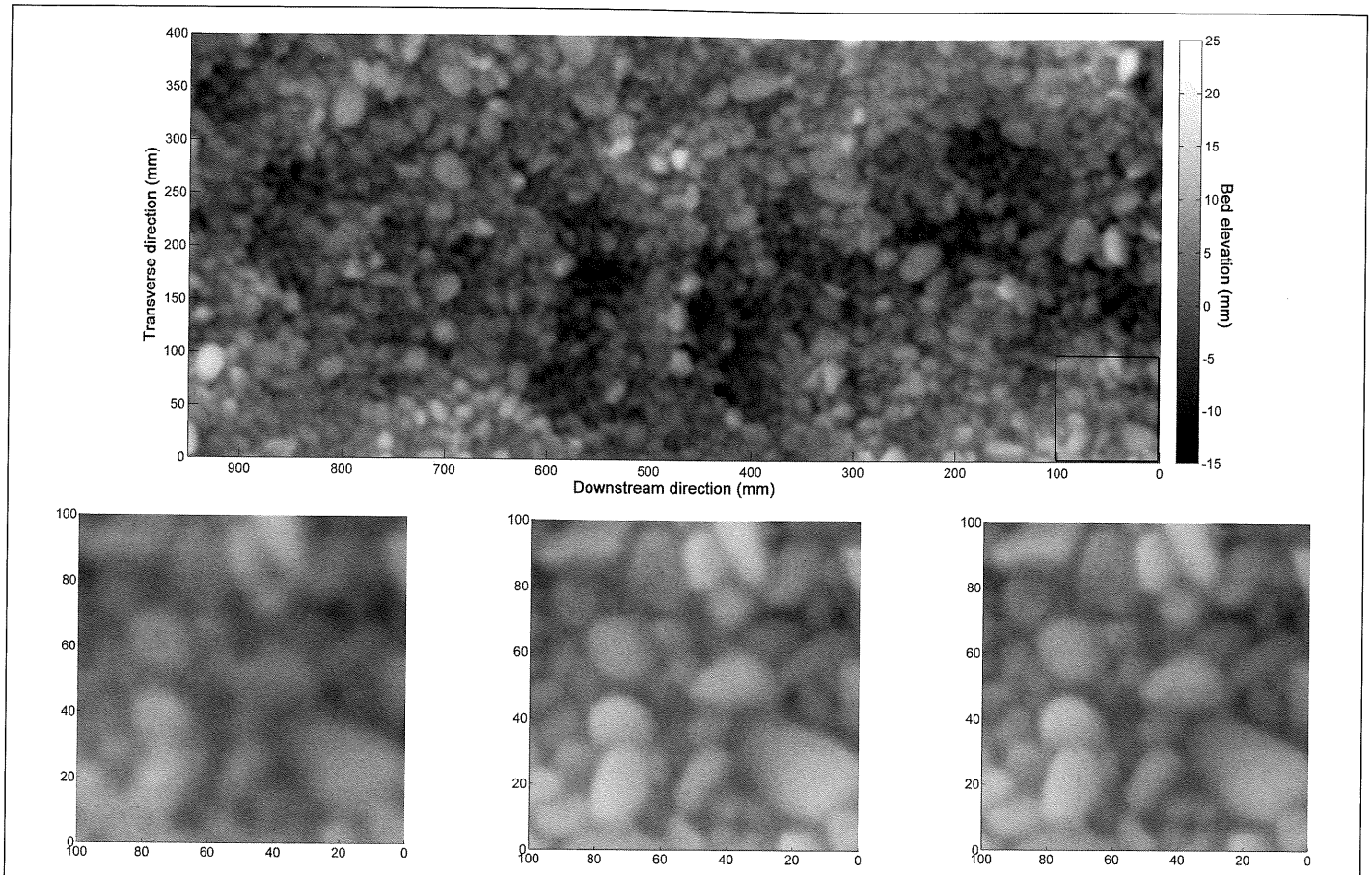

Figure 9. (Top) DEM of the full test section obtained at once (no merging), represented on a grid with 1 mm spacing; the theoretical depth resolution is 1·15 mm. (Bottom) Close-ups on bed structure without DEM merging (left); with DEM merging and resampled to 1 mm sampling distance (middle); with DEM merging and 0·25 mm sampling distance (right).

compared to the merged DEM (Figure 5). Small gravel particles are hardly distinguishable in the non-merged DEM. It is suited for general bed-roughness analysis, but analysis on the relationship between detailed grain roughness and bed roughness is not possible with the non-merged DEM. Visually, no differences are distinguishable between merged DEMs resampled at 0·25 mm and 1 mm, respectively, which agrees well with our analysis as presented in Figure 4.

The non-merged DEM was compared with the composite DEM obtained using merging. No particular trend was observed in the DEM of Difference (DoD), outside from a reduced sharpness of the non-merged DEM at the edges and gaps between gravel particles. For this reason, we solely report the results of the quantitative evaluation. The difference between the two DEMs was characterized by a MUE of 1·30 mm and a SDE of 1·68 mm globally over the test section. This represents the internal reliability of the non-merged DEM. One can see that DEM quality is considerably degraded compared with the composite DEM obtained from the merging of three individual DEMs of better quality.

The last step in our evaluation of the merging method examined the effect of scale variation, to simulate the merging of coarser data with higher uncertainties (e.g., data collected from aerial platforms). For the tests, the DEMs' sampling distance was degraded by a factor of 2 and 4, resulting in new DEM grid sizes of 2 mm and 4 mm, respectively. Degraded DEMs were registered and merged the same way as the original DEMs, which were characterized by a 1 mm sampling distance. The fundamental difference being that the precision of the horizontal alignment was changed from 1 mm to 2 mm and 4 mm for the two cases studied, respectively, since the horizontal registration precision equals the DEM grid size (see the "3D Co-Registration and Merging" Section). Figure 10 shows the residual maps after co-registration of DEM-1 and DEM-2, for the two new DEM grid sizes. One can see the large systematic errors resulting from the change in horizontal registration precision, especially for the 4 mm case. This is because the position of the stitching line was offset by 1 mm and 3 mm compared with the optimum position detected using the 1 mm resolution DEMs, for the 2 mm and 4 mm cases, respectively. Resulting from the inaccurate horizontal alignment, seamless merging failed and the residual maps were characterized by a MUE = 1.04 mm (SDE = 1.47 mm) and MUE = 1.88 mm (SDE = 2.47 mm), for the 2 mm and 4 mm cases, respectively, compared with MUE = 0.67 mm (SDE = 1.02 mm) obtained using the original resolution of 1 mm (Figure 7).

It is clear that the decision on which DEM grid size to choose (hence on the horizontal alignment precision) is critical for effective merging. Coarse DEM merging can be improved by resampling the DEMs onto finer grids, hence improving the horizontal alignment precision, before co-registration. After merging, the unnecessary high-resolution DEM can be transformed back to its original sampling distance. When there is no *a-priori* knowledge of the optimum registration resolution, this can be determined by error and trial, until effective seamless merging is achieved. Here, the degraded DEMs characterized by grid spacing of 2 mm and 4 mm, respectively, were resampled onto the original 1 mm grid, before merging. This enabled detection of the optimum stitching line, and thus satisfied the condition of seamless merging (Figure 10).

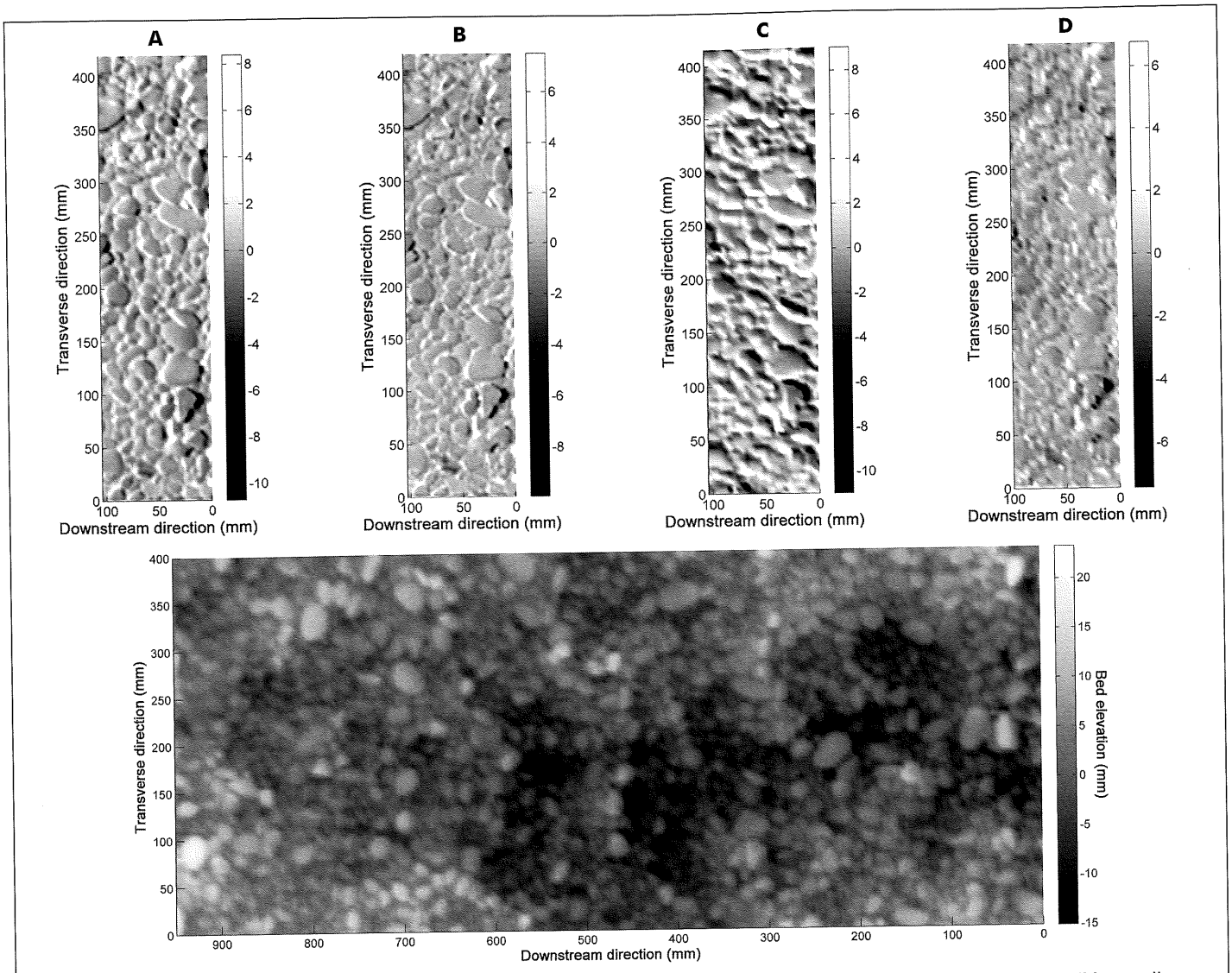

Figure 10. Residual maps, i.e., elevation difference in mm between DEM-1 and DEM-2 after co-registration, for (A, B) a DEM sampling distance of 2 mm; and (C, D) a DEM sampling distance of 4 mm; (A, C) The horizontal alignment precision equaled the DEM sampling distance; and (B, D) the horizontal alignment precision was 1 mm to improve DEM co-registration. Below is the final DEM after merging. The sampling distance is 4 mm, while the horizontal alignment was performed with DEMs resampled on 1 mm grids prior to merging.

Discussion and Conclusions

The results presented herewith indicate that the natural trade-off between measurement resolution and surface coverage encountered with digital photogrammetry and other remote sensing techniques can be overcome by merging overlapping DEMs. The presented merging approach can easily be integrated in our stereo-photogrammetric DEM collection workflow (Bertin *et al.*, 2015). We present how future merging must be considered during the design stage, by identifying the measurement resolution needed for future grain-scale analysis, and then calculating the number of DEMs needed to cover the region of interest. During the design stage, the size of the overlap between adjacent DEMs needs to be considered. It is clear that the choice of overlap affects the merging potential, although only limited detailed past research on overlap dimensions is available. Our preliminary tests suggested 30 percent to be a good compromise between data redundancy and data handling, a value which was also reported in previous studies (e.g., Marzahn *et al.* (2012)). We provide information on a best-fit approach to accurately undertake 3D co-registration of individual DEMs, using the least-squares method and standard averaging of overlapping elevations, to ensure seamless merging.

Our merging methodology can be adapted to DEMs collected using any measurement technique, as long as a DEM overlap is accounted for and measured elevations are arranged on a regular grid (unlike non-gridded point cloud data). The former was already identified as a natural pre-requisite for effective DEM merging (see the State of the Art section), while the latter is custom practice in the Earth sciences (Bouratsis *et al.*, 2013; Chandler *et al.*, 2002; Chandler *et al.*, 2001; Hodge *et al.*, 2009; Stojic *et al.*, 1998; Tarolli, 2014). A feature of interest, which is not investigated herewith, is the extent to which the co-registration process is able to align DEMs collected from very different viewpoints (e.g., when the setup is rotated substantially between the acquisitions of successive DEMs). For the present study it is not deemed applicable due to the vertical nature of the used measurements.

Previous studies (Bertin *et al.*, 2014; Hodge *et al.*, 2009) interpolated raw point clouds onto grids with spacing closely matching the original point data spacing, in order to reduce smoothing artifacts. Here, we show that the computational

expense during merging is reduced dramatically by resampling individual DEMs onto coarser grids before merging. Only minimal information will be lost. In our case, we compared 1 mm spacing for both merged and non-merged DEMs with 0·25 mm spacing of an individual DEM. In future, effective DEM resampling will become more important for fit-for-purpose analysis in order not to burden processing units with increasingly detailed data.

Our merging methodology was tested on DEMs of various geometric resolutions, in order to examine the effect of scale variation, since research in a variety of fields now use DEMs covering a range of spatial scales. The DEM sampling distance was shown to exert significant control on the DEM co-registration, and thus merging performance. Merging coarse DEMs improved by resampling DEMs onto finer grids, hence improving the DEM alignment precision, prior to DEM co-registration. If done appropriately, it is shown that the merging method presented is able to handle a range of spatial scales.

Although we only presented merging of DEMs along one axis, our technique can be applied for DEM merging in both the lateral and longitudinal directions. In field applications, where the measurement area is generally larger than in the laboratory, we expect DEM merging to soon become a common application, allowing analyzing fluvial surfaces at different scales, from the grain scale to larger bedforms and channel shape. The merging process will not differ from the laboratory application presented herewith. However, extra difficulty resides in ensuring adequate overlap and consistent viewing geometry throughout the acquisition of the successive stereo pairs. In the laboratory, this was achieved by moving the setup along a straight rail over a distance set by the overlap and camera-height (see Figure 2). For *in-situ* deployment, DEM co-registration shall be improved by accounting for any roll of the setup around the vertical axis. This can be efficiently performed with MATLAB® by applying a solid rotation to the DEMs prior to merging. The overlap distance can be noted directly on the ground by using fixed markers.

We currently further develop our stereo-photogrammetric solution by identifying the minimum area of DEM overlap, allowing for accurate co-registration, and a more detailed evaluation of suitable averaging methods. Residual maps between overlapping DEMs show differences in the occluded regions, the particles' edges and gaps (Figure 7), and we expect that merged DEMs with weighted-averaging, for example with weights depending on the DEM cells' aspect angle, can improve the DEM quality in those occluded regions, beyond the quality of individual DEMs.

Acknowledgments

The authors would like to thank the Editor-in-Chief, Dr. Russell G. Congalton, and the anonymous reviewers for their valuable comments, which helped to improve the paper.

References

Barazzetti, L., M.Previtali, and M. Scaioni, 2013. Stitching and processing gnomonic projections for close-range photogrammetry, *Photogrammetric Engineering & Remote Sensing*, 79(6):573–582.

Bertin, S., and H. Friedrich, 2014. Measurement of gravel-bed topography: Evaluation study applying statistical roughness analysis, *Journal of Hydraulic Engineering*, 140(3):269–279.

Bertin, S., H. Friedrich, P. Delmas, and E. Chan, 2013. The use of close-range digital stereo-photogrammetry to measure gravel-bed topography in a laboratory environment, *Proceedings of the 35th IAHR Congress*, Chengdu, China, unpaginated CD-ROM.

Bertin, S., H. Friedrich, P. Delmas, E. Chan, and G. Gimel'farb, 2014. DEM quality assessment with a 3D printed gravel bed applied to stereo photogrammetry, *The Photogrammetric Record*, 29(146):241–264.

Bertin, S., H. Friedrich, P. Delmas, E. Chan, and G. Gimel'farb, 2015. Digital stereo photogrammetry for grain-scale monitoring of fluvial surfaces: Error evaluation and workflow optimisation, *ISPRS Journal of Photogrammetry and Remote Sensing*, 101(0):193–208.

Bouguet, J.-Y., 2010. Camera Calibration Toolbox for Matlab®, URL: *http://www.vision.caltech.edu/bouguetj/calib_doc/*, (last date accessed, 16 November 2015).

Bouratsis, P., P. Diplas, C.L. Dancey, and N. Apsilidis, 2013. High-resolution 3D monitoring of evolving sediment beds, *Water Resources Research*, 49(2):977–992.

Bruno, F., G. Bianco, M. Muzzupappa, S. Barone, and A.V. Razionale, 2011. Experimentation of structured light and stereo vision for underwater 3D reconstruction, *ISPRS Journal of Photogrammetry and Remote Sensing*, 66(4):508–518.

Butler, J.B., S.N. Lane, and J.H. Chandler, 2001. Characterization of the structure of river-bed gravels using two-dimensional fractal analysis, *Mathematical Geology*, 33(3):301–330.

Chandler, J., P. Ashmore, C. Paola, M. Gooch, and F. Varkaris, 2002. Monitoring river-channel change using terrestrial oblique digital imagery and automated digital photogrammetry, *Annals of the Association of American Geographers*, 92(4):631–644.

Chandler, J., K. Shiono, P. Rameshwaran, and S. Lane, 2001. Measuring flume surfaces for hydraulics research using a Kodak DCS460, *The Photogrammetric Record*, 17(97):39–61.

Costantini, M., F. Malvarosa, F. Minati, E. Zappitelli, and F.M. Seifert, 2006. A data fusion algorithm for DEM mosaicking: Building a global DEM with SRTM-X and ERS data, *Proceedings of the IEEE International Geoscience and Remote Sensing Symposium*, Denver, Colorado, pp. 3861–3864.

Dowling, T.I., A. Read, and J.C. Gallant, 2009. Very high resolution DEM acquisition at low cost using a digital camera and free software, *Proceedings of the 18th World IMACS Congress and MODSIM09 International Congress on Modelling and Simulation*, Cairns, Australia, pp. 2479–2485.

Fonstad, M.A., J.T. Dietrich, B.C. Courville, J.L. Jensen, and P.E. Carbonneau, 2013. Topographic structure from motion: A new development in photogrammetric measurement, *Earth Surface Processes and Landforms*, 38(4):421–430.

Fusiello, A., E. Trucco, and A.Verri, 2000. A compact algorithm for rectification of stereo pairs, *Machine Vision and Applications*, 12(1):16–22.

Gallant, J. C., and J.M. Austin, 2009. Stitching fine resolution DEMs, *Proceedings of the the 18th World IMACS Congress and MODSIM09 International Congress on Modelling and Simulation*, Cairns, Australia, Modelling and Simulation Society of Australia and New Zealand and International Association for Mathematics and Computers in Simulation, pp. 2486–2492.

Gesch, D., and R. Wilson, 2002. Development of a seamless multisource topographic/ bathymetric elevation model of Tampa Bay, *Marine Technology Society Journal*, 35(4):58–64.

Gimel'farb, G., 2002. Probabilistic regularisation and symmetry in binocular dynamic programming stereo, *Pattern Recognition Letters*, 23(4):431–442.

Heays, K.G., H. Friedrich, and B.W. Melville, 2014. Laboratory study of gravel-bed cluster formation and disintegration, *Water Resources Research*, 50(3):2227–2241.

Hodge, R., J. Brasington, and K. Richards, 2009. In situ characterization of grain-scale fluvial morphology using Terrestrial Laser Scanning, *Earth Surface Processes and Landforms*, 34(7):954–968.

James, M.R., and S. Robson, 2014. Sequential digital elevation models of active lava flows from ground-based stereo time-lapse imagery, *ISPRS Journal of Photogrammetry and Remote Sensing*, 97(0):160–170.

James, T.D., P.E. Carbonneau, and S.N. Lane, 2007. Investigating the effects of DEM error in scaling analysis, *Photogrammetric Engineering & Remote Sensing*, 73(1):67–78.

Javernick, L., J. Brasington, and B. Caruso, 2014. Modeling the topography of shallow braided rivers using Structure-from-Motion photogrammetry, *Geomorphology*, 213:166–182.

Marzahn, P., D. Rieke-Zapp, and R. Ludwig, 2012. Assessment of soil surface roughness statistics for microwave remote sensing applications using a simple photogrammetric acquisition system, *ISPRS Journal of Photogrammetry and Remote Sensing*, 72(0):80–89.

Medeiros, S.C., T. Ali, S.C. Hagen, and J.P. Raiford, 2011. Development of a seamless topographic/bathymetric digital terrain model for Tampa bBay, Florida, *Photogrammetric Engineering & Remote Sensing*, 77(12):1249–1256.

Musumeci, R., G. Farinella, E. Foti, S. Battiato, T. Petersen, and B.M. Sumer, 2013. Measuring sandy bottom dynamics by exploiting depth from stereo video sequences, *Proceedings of Image Analysis and Processing - ICIAP 2013* (A. Petrosino, editor), Springer, Berlin, pp. 420–430.

Ouédraogo, M.M., A. Degré, C. Debouche, and J. Lisein, J., 2014. The evaluation of unmanned aerial system-based photogrammetry and terrestrial laser scanning to generate DEMs of agricultural watersheds, *Geomorphology*, 214(0):339–355.

Papasaika, H., E. Kokiopoulou, E. Baltsavias, K. Schindler, and D. Kressner, 2011. Fusion of digital elevation models using sparse representation, *Photogrammetric Image Analysis, Lecture Notes on Computer Science, 6952* (Stilla U., F. Rottensteiner, H. Mayer, B. Jutzi, and M. Butenuth, editors), Springer, Berlin, 317:171–84.

Papasaika, H., D. Poli, and E. Baltsavias, 2008. A framework for the fusion of digital elevation models, *Proceedings of the ISPRS Congress - Beijing 2008*, Beijing, China, pp. 811–818.

Schindler, K., H. Papasaika, S. Schutz, S., and E. Baltsavias, 2011. Improving wide-area DEMs through data fusion - Chances and limits, *Proceedings of the 53rd Photogrammetric Week*, Stuttgart, Germany, pp. 159–170.

Stojic, M., J. Chandler, P. Ashmore, and J. Luce, 1998. The assessment of sediment transport rates by automated digital photogrammetry, *Photogrammetric Engineering & Remote Sensing*, 64(5):387–395.

Streutker, D.R., N.F. Glenn, and R. Shrestha, 2011. A slope-based method for matching elevation surfaces, *Photogrammetric Engineering & Remote Sensing*, 77(7):743–750.

Stumpf, A., J.P. Malet, P. Allemand, M. Pierrot-Deseilligny, and G. Skupinski, 2015. Ground-based multi-view photogrammetry for the monitoring of landslide deformation and erosion, *Geomorphology*, 231(0):130–145.

Tarolli, P., 2014. High-resolution topography for understanding Earth surface processes: Opportunities and challenges, *Geomorphology*, 216(0):295–312.

Tran, T.A., V. Raghavan, S. Masumoto, P. Vinayaraj, and G. Yonezawa, 2014. A geomorphology-based approach for digital elevation model fusion - Case study in Danang City, Vietnam, *Earth Surface Dynamics*, 2(2):403–417.

Wackrow, R., 2008. *Spatial Measurement with Consumer Grade Digital Cameras*, Ph.D.
dissertation, Loughborough University, Loughborough, UK, 241 p.

Westoby, M.J., J. Brasington, N.F. Glasser, M.J. Hambrey, and J.M. Reynolds, 2012. 'Structure-from-Motion' photogrammetry: A low-cost, effective tool for geoscience applications, *Geomorphology*, 179(0):300–314.

(Received 11 March 2015; accepted 10 July 2015; final version 13 July 2015)